J|A|C|S COMMUNICATIONS

Published on Web 02/26/2010

Core-Expanded Naphthalene Diimides Fused with 2-(1,3-Dithiol-2-Ylidene)Malonitrile Groups for High-Performance, Ambient-Stable, Solution-Processed n-Channel Organic Thin Film Transistors

Xike Gao,*[,†] Chong-an Di,*[,‡] Yunbin Hu,[†] Xiaodi Yang,[§] Hongyu Fan,[†] Feng Zhang,[†] Yunqi Liu,[‡] Hongxiang Li,[†] and Daoben Zhu*[‡,†]

Laboratory of Materials Science, Shanghai Institute of Organic Chemistry, Chinese Academy of Sciences (CAS), 345 Lingling Road, Shanghai 200032, China, Beijing National Laboratory for Molecular Sciences, Key Laboratory of Organic Solids, Institute of Chemistry, CAS, Beijing 100190, China, and Laboratory of Advanced Materials, Fudan University, Shanghai 200433, China

Received December 18, 2009; E-mail: gaoxk@mail.sioc.ac.cn; dicha@iccas.ac.cn

Driven by the demand for low-cost, large-area, and flexible organic electronic devices, organic complementary circuits comprising both p- and n-channel organic thin film transistors (OTFTs) are attracting ever increasing attention due to their low power dissipation, high operating speed, and good noise margin.[1] Although some solution-processed p-channel OTFTs have shown hole mobilities ≥ 1.0 cm^2 V^{-1} s^{-1} with good ambient stability,[2] the distinct lack of high-performance, ambient-stable, solution-processed n-channel OTFTs has hindered the development of low-cost organic complementary circuits.[3] Therefore, the development of reliable n-channel organic semiconductors is a crucial issue in organic electronics.

Naphthalene diimides (NDIs) and perylene diimides (PDIs) are among the best n-channel organic semiconductors,[4] and their ambient-stable OTFT devices, fabricated by thermal evaporation, show a high electron mobility of up to 0.57 and 1.24 cm^2 V^{-1} s^{-1}, respectively.[5] However, the electron mobilities of solution-processed NDI- and PDI-based OTFTs are limited to $\sim$0.1 cm^2 V^{-1} s^{-1}.[4a,6] Recently, a high-mobility electron-transporting donor−acceptor polymer P(NDI2OD-T2), containing NDI and bithiophene repeat units, was reported by Facchetti and co-workers.[7] When this polymer was used for solution fabrication of top-gate bottom-contact OTFTs, the devices exhibited a high electron mobility of up to 0.85 cm^2 V^{-1} s^{-1} under ambient conditions. These results indicate that the synthesis of excellent n-type organic semiconductors is possible through the chemical modification of NDI cores.

Müllen et al.[8] performed pioneering work on core-expanded perylene diimides by chemically modifying PDI cores. While investigations of core-extended NDIs are far less common, our previous work on tetrabromonaphthalene diimide (TBNDI) opens up new opportunities for the synthesis of core-expanded NDIs.[9] In addition, Yamashita et al.[10] demonstrated that 2-(1,3-dithiol-2-ylidene)malonitrile, when fused with quinones, provides acceptors that are more electron-deficient than chloranil. Therefore, we envision that the core-expanded NDI derivatives bearing two 2-(1,3-dithiol-2-ylidene)malonitrile moieties at the central naphthalene core, as shown in Figure 1, are promising n-type organic semiconductors. There are two reasons for this molecular design: (i) the expanded planar π-conjugation promotes intermolecular $\pi-\pi$ stacking, which is crucial for obtaining high electron mobility; and (ii) the large degree of π-electron deficiency imparted by the malonitrile-based moieties can depress LUMO energies, which is important for realizing electron injection and conduction with

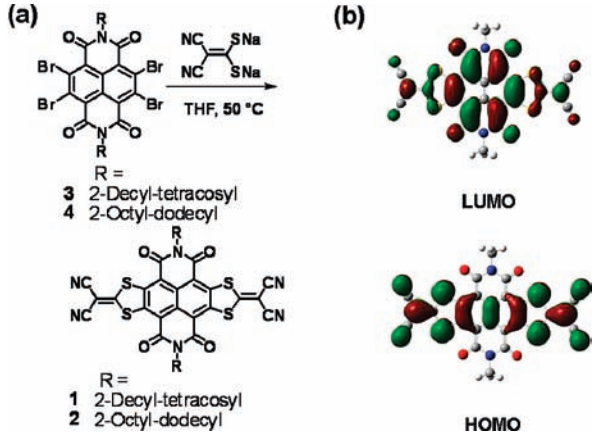

Figure 1. (a) Synthesis of core-expanded NDIs fused with 2-(1,3-dithiol-2-ylidene)malonitrile groups (**1** and **2**). (b) HOMO/LUMO levels of a N,N′-bis(methyl)-substituted model molecule used to calculate the theoretical molecular orbitals of **1** and **2**.

ambient stability. Herein, we report on the first two representative compounds, both bearing long branched N-alkyl chains (Figure 1a, **1** and **2** with R = 2-decyl-tetracosyl and 2-octyl-dodecyl, respectively). **1** and **2** have good solubility in common organic solvents, and their solution-processed OTFTs, operating under ambient conditions, exhibit high electron mobilities of up to 0.51 cm^2 V^{-1} s^{-1}. To the best of our knowledge, these electron mobilities are among the highest values reported for solution-processed, ambient-stable n-channel OTFT devices and are higher than the performance of P(NDI2OD-T2)-based OTFTs (0.01 cm^2 V^{-1} s^{-1}) having the same device configuration.[7]

As shown in Figure 1a, compounds **1** and **2** were readily synthesized by the nucleophilic aromatic substitution reaction of the corresponding TBNDI (**3** or **4**) and sodium 1,1-dicyanoethylene-2,2-dithiolate[11] (see Supporting Information for details). At room temperature, **1** and **2** are highly soluble in $CHCl_3$, CH_2Cl_2, and THF (>10 mg/mL) and less soluble in toluene and dichlorobenzene. Thermogravimetric analysis (TGA) and differential scanning calorimetry (DSC) analyses show that the thermolysis onset temperatures for **1** and **2** are both 386 °C, with high melting points at 242 and 265 °C, respectively (see Figures S1−S4 in the Supporting Information). The TGA and DSC results therefore indicate that **1** and **2** are thermally stable, which allows analysis of thin film crystallinity and microstructure over a broad range of annealing temperatures, from room temperature to $\sim$220 °C.

To estimate the position and energies of frontier orbitals for **1** and **2**, Density Functional Theory (DFT) calculations were per-

[†] Shanghai Institute of Organic Chemistry.
[‡] Institute of Chemistry.
[§] Fudan University.

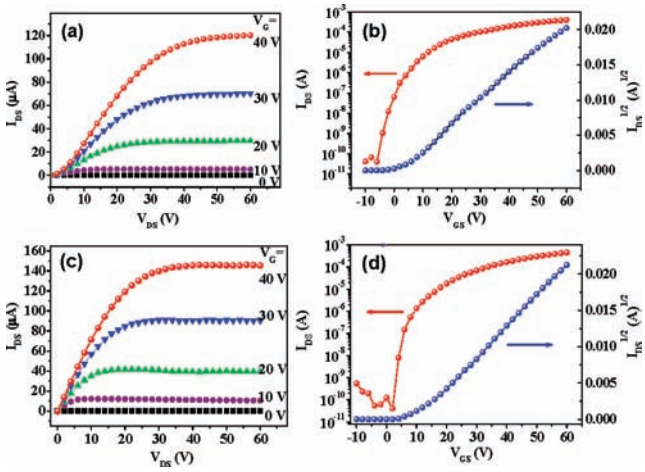

Figure 2. $I_{DS}-V$ plots for OTFT devices fabricated by spin coating of **2** on OTS-treated substrate annealing at 180 °C, measured under ambient conditions: Output characteristics and transfer characteristics at $V_{DS} = 60$ V for an Au-contact device (a, b) and an Ag-contact device (c, d).

formed using the Gaussian 03 program at the B3LYP/6-31G(d) level. N-Alkyl chains were replaced by N-methyl groups in calculations to reduce the time required for calculation. This substitution should not affect the calculations because the influence of N-alkyl chains on the electron structure of the molecule is considered negligible. As shown in Figure 1b, the largest coefficients in the HOMO orbital are located on the entire lateral axis π-system, and the coefficients in the LUMO orbital are mainly positioned on the central NDI unit. The energy values of the HOMO and LUMO orbitals of **1** (or **2**) were also estimated by DFT (HOMO: −6.8 eV; LUMO: −4.5 eV; band gap: 2.3 eV). Compared to the frontier orbitals of unsubstituted NDI (HOMO: −7.0 eV; LUMO: −3.4 eV; band gap: 3.6 eV),[9a] **1** and **2** have a slightly higher HOMO level, a much lower-lying LUMO level, and a narrower band gap.

The absorption spectra of **1** and **2** in CH_2Cl_2 are nearly identical with the maximum end absorption band at 578 nm. Their thin-film absorbances are red-shifted (to 594 and 597 nm for **1** and **2**, respectively, Figure S5), indicating that intermolecular $\pi-\pi$ stacking is present in the solid state. Optical energy gaps (E_g^{opt}) for **1** and **2**, estimated from the onset of absorption in the solution and film, are 2.1 and 2.0 eV, respectively. These gaps are comparable to the aforementioned DFT calculated value (2.3 eV). **1** and **2** exhibit nearly identical solution cyclic voltammetric (CV) behaviors in CH_2Cl_2, with two reversible reductions (Figure S6), in which the first half-wave potential ($E_{1/2}^{red1}$) is at approximately −0.1 V. The LUMO energies of **1** and **2**, estimated by CV ($E_{LUMO} = -(E_{1/2}^{red1} + 4.44)$ eV),[12] are both at −4.3 eV, which is consistent with the calculated value (−4.5 eV). The low-lying LUMO levels of **1** and **2** are crucial for achieving ambient-stable electron injection and conduction in their respective OTFT devices.[4c,5b]

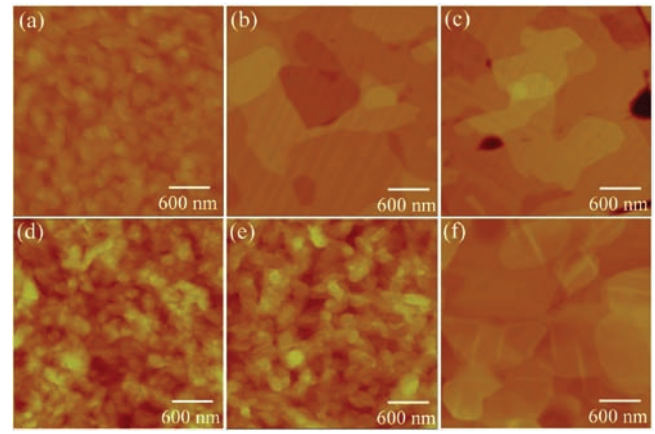

Figure 3. AFM images of thin films of **1** (a, annealed at 120 °C; b, annealed at 160 °C; c, annealed at 180 °C) and **2** (d, annealed at 120 °C; e, annealed at 160 °C; f, annealed at 180 °C).

Thin films (40−60 nm in thickness) of **1** and **2** were spin-coated on octadecyltrichlorosilane (OTS)-treated SiO_2/Si substrates. Next, the thin films were annealed at 120, 160, or 180 °C. Au (or Ag) source/drain contacts (30 nm in thickness) were deposited on the organic layer through a shadow mask, affording a bottom-gate top-contact device configuration. All devices were tested in air. Figure 2 shows the device characteristics of **2** (see Figure S8 for the device characteristics of **1**). The device performances of **1** and **2** are summarized in Table 1. All devices exhibit a high electron mobility and good current modulation under ambient conditions. In addition, the devices exhibit high current on/off ratios of 10^5-10^7 and low threshold voltages ($V_T < 6$ V for Au-contact devices, $V_T < 9$ V for Ag-contact devices).

The as-spun (unannealed) thin film devices based on **1** and **2** show a relatively low electron mobility (~10^{-2} cm^2 V^{-1} s^{-1}). Thermal annealing of the devices has a different effect on device performance. Devices based on **1** and annealed at 160 °C show an enhanced electron mobility of 0.11−0.20 cm^2 V^{-1} s^{-1} relative to those annealed at 120 °C (0.07−0.12 cm^2 V^{-1} s^{-1}). This positive effect is ascribed to the improved thin film morphology (the increased grain size and the decreased grain boundaries), which is revealed by atomic force microscopy (AFM) images (Figure 3a and 3b). However, the device performance was not further enhanced when a thin film of **1** was annealed at 180 °C (with a moderate mobility of 0.10−0.15 cm^2 V^{-1} s^{-1}). When subjected to annealing temperatures ranging from 120 to 180 °C, the electron mobility of devices based on **2** showed a stepwise and significant improvement ($\mu_e = 0.08-0.14$ cm^2 V^{-1} s^{-1} at 120 °C; $\mu_e = 0.15-0.25$ cm^2 V^{-1} s^{-1} at 160 °C; and $\mu_e = 0.29-0.42$ cm^2 V^{-1} s^{-1} at 180 °C). The explanation for the temperature-related enhancement of the device performance of **2** can be found using X-ray diffraction (XRD) and AFM studies. XRD studies show that, with increasing annealing temperature, the intensity of reflection peaks is enhanced and the

Table 1. Maximum (Average) Electron Mobilities (μ_e), Threshold Voltages (V_T), and Current On/Off Ratios (I_{on}/I_{off}) for Devices Based on **1** and **2** Fabricated by Spin Coating on OTS-Treated SiO_2/Si Substrates and Annealed at 120, 160, and 180 °C

		Annealed at 120 °C			Annealed at 160 °C			Annealed at 180 °C		
	Source/Drain Electrodes	μ_e[a] (cm^2 V^{-1} s^{-1})	V_T[a] (V)	I_{on}/I_{off}[a]	μ_e[a] (cm^2 V^{-1} s^{-1})	V_T[a] (V)	I_{on}/I_{off}[a]	μ_e[a] (cm^2 V^{-1} s^{-1})	V_T[a] (V)	I_{on}/I_{off}[a]
1	Au	0.12(0.09)	−2−4	10^5-10^6	0.20(0.15)	−2−5	10^5-10^6	0.15(0.14)	−4−1	10^5-10^6
1	Ag[b]				0.20(0.14)	0−8	10^5-10^6			
2	Au	0.14(0.10)	−1−6	10^5-10^6	0.25(0.20)	−2−3	10^5-10^6	0.42(0.32)	0−5	10^5-10^7
2	Ag[b]							0.51(0.43)	2−9	10^6-10^7

[a] Typical device characteristics obtained from more than 10 devices; all devices were measured under ambient conditions. [b] Only thin films of **1** annealed at 160 °C and those of **2** annealed at 180 °C were fabricated and measured for Ag-contact devices.

peaks become sharper, with fourth- and fifth-order reflection peaks visible (see Figure S7 for XRD spectra). These data indicate that lamellar ordering and crystallinity on the substrate are improved. AFM images (Figure 3d−f) of thin films of **2** show visible changes along with increasing annealing temperature, the grain size increases (100−300 nm at 120 °C; 200−600 nm at 160 °C; 800−2500 nm at 180 °C), and the grain boundaries decrease. Therefore, the enhanced lamellar ordering of the thin film and the increased grain size explain the improved device performance of **2**. It should be noted that the devices based on **2** show higher electron mobilities than those based on **1**. This phenomenon indicates that the nature of the N-alkyl chains of **1** and **2** influence their device performance.

Large contact resistance, as indicated by the S-shaped output characteristics at low source−drain voltages (Figure 2a), can be observed. The contact resistance is mainly attributed to the large injection barrier of 0.8 eV between Au and **2**. The transfer characteristics shown in Figure 2b reveal the device performance with $\mu_e = 0.36$ cm^2 V^{-1} s^{-1}, $I_{on}/I_{off} = 10^7$ and $V_T = 4.2$ V for an Au-contact device based on **2** (annealed at 180 °C). The implementation of low work function electrodes can minimize the energy barrier for electron injection from the electrode to the LUMO of organic semiconductors, and this plays an important role in improving device performance.[13] When the Ag-source/drain electrodes were used in place of Au, the S-shaped output characteristics disappeared (Figure 2c), indicating a lower contact resistance between the Ag electrode and the semiconductor. This also resulted in a significantly improved performance, with $\mu_e = 0.45$ cm^2 V^{-1} s^{-1}, $I_{on}/I_{off} = 10^7$, and $V_T = 8.5$ V for a 180 °C annealed device based on **2** (Figure 2c and 2d).[14] These devices based on **2** with Ag contacts (annealed at 180 °C) afford the highest electron mobility of 0.51 cm^2 V^{-1} s^{-1} (Figure S9), which is the best device performance reported to date for solution-processed, n-type small organic molecule-based devices operating under ambient conditions. It should be noted that the Au-contact devices operated under an inert atmosphere were comparable in performance to those tested under ambient conditions. Moreover, Au-contact devices based on **2** show excellent air stability over a period of 5 weeks, with a nearly identical electron mobility of 0.3 cm^2 V^{-1} s^{-1}, a stable current on/off ratio of 10^6, and a minimally shifted threshold voltage below 5 V (Figures S10 and S11). The **2**-based Au-contact devices also exhibit satisfactory operating stability during the cycle test (5000 times, Figure S12). The excellent air stability of the device is attributed to the combination of the low-lying LUMO levels (−4.3 eV) of the organic semiconductor, its good crystallinity, and the smooth interconnected thin film morphology.[5b,15]

In conclusion, we have developed a new class of n-type organic semiconductors, based on core-expanded naphthalene diimides fused with 2-(1,3-dithiol-2-ylidene)malonitrile groups. The first two representatives of these species, **1** and **2**, derived from long branched N-alkyl chains have been used successfully as active layers for high-performance, ambient-stable, solution-processed n-channel organic thin film transistors. The fabricated devices exhibit high electron mobilities of up to 0.51 cm^2 V^{-1} s^{-1}, with current on/off ratios of 10^5−10^7, and threshold voltages below 10 V under ambient conditions. Moreover, their excellent air and operating stability warrant their great potential in organic electronics.

Acknowledgment. This research was financially supported by the Shanghai Natural Science Foundation (09ZR1438500), the National Natural Science Foundation (20902105 and 60901050), and the Chinese Academy of Sciences.

Supporting Information Available: Synthesis and characterizations of compounds **1** and **2**, and details concerning OTFT device fabrication/characterization. This material is available free of charge via the Internet at http://pubs.acs.org.

References

(1) (a) Meijer, E. J.; de Leeuw, D. M.; Setayesh, S.; van Veenendaal, E.; Huisman, B.-H.; Blom, P. W. M.; Hummelen, J. C.; Scherf, U.; Klapwijk, T. M. *Nat. Mater.* **2003**, *2*, 678–682. (b) Klauk, H.; Zschieschang, U.; Pflaum, J.; Halik, M. *Nature* **2007**, *445*, 745–748.

(2) (a) Payne, M. M.; Parkin, S. R.; Anthony, J. E.; Kuo, C.-C.; Jackson, T. N. *J. Am. Chem. Soc.* **2005**, *127*, 4986–4987. (b) Ebata, H.; Izawa, T.; Miyazaki, E.; Takimiya, K.; Ikeda, M.; Kuwabara, H.; Yui, T. *J. Am. Chem. Soc.* **2007**, *129*, 15732–15733. (c) Subramanian, S.; Park, S. K.; Parkin, S. R.; Podzorov, V.; Jackson, T. N.; Anthony, J. E. *J. Am. Chem. Soc.* **2008**, *130*, 2706–2707. (d) Gao, P.; Beckmann, D.; Tsao, H. N.; Feng, X.; Enkelmann, V.; Baumgarten, M.; Pisula, W.; Müllen, K. *Adv. Mater.* **2009**, *21*, 213–216. (e) Hamilton, R.; Smith, J.; Ogier, S.; Heeney, M.; Anthony, J. E.; McCulloch, I.; Veres, J.; Bradley, D. D. C.; Anthopoulos, T. D. *Adv. Mater.* **2009**, *21*, 1166–1171.

(3) (a) Newman, C. R.; Frisbie, C. D.; da Silva Filho, D. A.; Brédas, J.-L.; Ewbank, P. C.; Mann, K. R. *Chem. Mater.* **2004**, *16*, 4436–4451. (b) Chua, L.-L.; Zaumseil, J.; Chang, J.-F.; Ou, E. C.-W.; Ho, P. K.-H.; Sirringhaus, H.; Friend, R. H. *Nature* **2005**, *434*, 194–199. (c) Oh, J. H.; Lee, H. W.; Mannsfeld, S.; Stoltenberg, R. M.; Jung, E.; Jin, Y. W.; Kim, J. M.; Yoo, J.-B.; Bao, Z. *Proc. Natl. Acad. Sci. U.S.A.* **2009**, *106*, 6065–6070. (d) Usta, H.; Risko, C.; Wang, Z.; Huang, H.; Deliomeroglu, M. K.; Zhukhovitskiy, A.; Facchetti, A.; Marks, T. J. *J. Am. Chem. Soc.* **2009**, *131*, 5586–5608.

(4) (a) Katz, H. E.; Lovinger, A. J.; Johnson, J.; Kloc, C.; Siegrist, T.; Li, W.; Lin, Y.-Y.; Dodabalapur, A. *Nature* **2000**, *404*, 478–481. (b) Jones, B. A.; Ahrens, M. J.; Yoon, M.-H.; Facchetti, A.; Marks, T. J.; Wasielewski, M. R. *Angew. Chem., Int. Ed.* **2004**, *43*, 6363–6366. (c) Jones, B. A.; Facchetti, A.; Wasielewski, M. R.; Marks, T. J. *J. Am. Chem. Soc.* **2007**, *129*, 15259–15278.

(5) (a) See, K. C.; Landis, C.; Sarjeant, A.; Katz, H. E. *Chem. Mater.* **2008**, *20*, 3609–3616. (b) Schmidt, R.; Oh, J. H.; Sun, Y.-S.; Deppisch, M.; Krause, A.-M.; Radacki, K.; Braunschweig, H.; Könemann, M.; Erk, P.; Bao, Z.; Würthner, F. *J. Am. Chem. Soc.* **2009**, *131*, 6215–6228.

(6) (a) Yan, H.; Zheng, Y.; Blache, R.; Newman, C.; Lu, S.; Woerle, J.; Facchetti, A. *Adv. Mater.* **2008**, *20*, 3393–3398. (b) Piliego, C.; Jarzab, D.; Gigli, G.; Chen, Z.; Facchetti, A.; Loi, M. A. *Adv. Mater.* **2009**, *21*, 1573–1576.

(7) (a) Yan, H.; Chen, Z.; Zheng, Y.; Newman, C.; Quinn, J. R.; Dötz, F.; Kastler, M.; Facchetti, A. *Nature* **2009**, *457*, 679–686. (b) Chen, Z.; Zheng, Y.; Yan, H.; Facchetti, A. *J. Am. Chem. Soc.* **2009**, *131*, 8–9.

(8) (a) Rohr, U.; Schlichting, P.; Böhm, A.; Gross, M.; Meerholz, K.; Bräuchle, C.; Müllen, K. *Angew. Chem., Int. Ed.* **1998**, *37*, 1434–1437. (b) Avlasevich, Y.; Müller, S.; Erk, P.; Müllen, K. *Chem.—Eur. J.* **2007**, *13*, 6555–6561.

(9) (a) Gao, X.; Qiu, W.; Yang, X.; Liu, Y.; Wang, Y.; Zhang, H.; Qi, T.; Liu, Y.; Lu, K.; Du, C.; Shuai, Z.; Yu, G.; Zhu, D. *Org. Lett.* **2007**, *9*, 3917–3920. (b) Suraru, S.-L.; Würthner, F. *Synthesis* **2009**, 1841–1845.

(10) Yamashita, Y.; Suzuki, T.; Saito, G.; Mukai, T. *J. Chem. Soc., Chem. Commun.* **1986**, 1489–1491.

(11) Gao, X.; Dou, J.; Li, D.; Dong, F.; Wang, D. *J. Mol. Struct.* **2005**, *733*, 181–186.

(12) (a) de Leeuw, D. M.; Simenon, M. M. J.; Brown, A. R.; Einerhand, R. E. F. *Synth. Met.* **1997**, *87*, 53–59. (b) Usta, H.; Facchetti, A.; Marks, T. J. *J. Am. Chem. Soc.* **2008**, *130*, 8580–8581.

(13) (a) Lee, T.-W.; Byun, Y.; Koo, B.-W.; Kang, I.-N.; Lyu, Y.-Y.; Lee, C. H.; Pu, L.; Lee, S. Y. *Adv. Mater.* **2005**, *17*, 2180–2184. (b) Wöbkenberg, P. H.; Bradley, D. D. C.; Kronholm, D.; Hummelen, J. C.; de Leeuw, D. M.; Cölle, M.; Anthopoulos, T. D. *Synth. Met.* **2008**, *158*, 468–472.

(14) The Ag-contact devices tested immediately in air afford are comparable in performance to those measured in inert atmosphere but subsequently suffered from slow performance degradation (in air) due to gradual oxidation of the Ag electrode, resulting in an up-shifted electrode work function and enlarged injection barrier: Kim, J. B.; Kim, C. S.; Kim, Y. S.; Loo, Y.-L. *Appl. Phys. Lett.* **2009**, *95*, 183301.

(15) (a) Ling, M.-M.; Erk, P.; Gomez, M.; Koenemann, M.; Locklin, J.; Bao, Z. *Adv. Mater.* **2007**, *19*, 1123–1127. (b) Weitz, R. T.; Amsharov, K.; Zschieschang, U.; Burghard, M.; Jansen, M.; Kelsch, M.; Rhamati, B.; van Aken, P. A.; Kern, K.; Klauk, H. *Chem. Mater.* **2009**, *21*, 4949–4954.

JA910667Y